Distance Distributions and Proximity Estimation Given Knowledge of the Heterogeneous Network Layout

Dionysis Xenakis, *Member, IEEE*, Lazaros Merakos, Marios Kountouris, *Senior Member, IEEE*, Nikos Passas, and Christos Verikoukis, *Senior Member, IEEE*

***Abstract*—Today's heterogeneous wireless network (HWN) is a collection of ubiquitous wireless networking elements (WNEs) that support diverse functional capabilities and networking purposes. In such a heterogeneous networking environment, proximity estimation will play a key role for the seamless support of emerging applications that span from the direct exchange of localized traffic between homogeneous WNEs (peer-to-peer communications) to positioning for autonomous systems using location information from the ubiquitous HWN infrastructure. Since most of the existing wireless networking technologies enable the direct (or indirect) estimation of the distances and angles between their WNEs, the integration of such spatial information is a natural solution for robustly handling the unprecedented demand for proximity estimation between the myriads of WNEs. In this paper, we develop an analytical framework that integrates existing knowledge of the HWN layout to enable proximity estimation between WNE supporting different radio access technologies (RATs). In this direction, we derive closed-form expressions for the distance distribution between two tagged WNEs given partial (or full) knowledge of the HWN topology. The derived expressions enable us to analyze how different levels of location-awareness affect the performance of proximity estimation between WNEs that are not necessarily capable of communicating directly. Optimal strategies for the deployment of WNEs, as means of maximizing the probability of successful proximity estimation between two WNEs of interest, are presented, and useful guidelines for the design of location-aware proximity estimation in the nowadays HWN are drawn.**

***Index Terms*—Proximity estimation, cluster process, multi-tier model, heterogeneous wireless networks.**

I. Introduction

OVER the past few years, wireless networks have been transformed from a set of single-tier operator-deployed circuit-switched systems, designed to support voice-centric services in wide geographical regions, to a set of multi-tier networking clusters of user-installed IP-based wireless networking elements (WNEs), designed to support heterogeneous communication capabilities and diverse networking requirements. The nowadays heterogeneous wireless network (HWN) is composed by tower-mounted cellular base stations (BSs) for providing wide area coverage (a.k.a. macrocells), user-deployed small-sized base stations for boosting the area spectral efficiency of the licensed spectrum [1] (e.g., femtocells), wireless local area network access points for enabling high-data rate connections to the Internet over the unlicensed spectrum [2], as well as other low-cost low-power and battery-operated sensors for monitoring, measuring, and communicating localized changes in nearby sink nodes [3], [4] (e.g., energy monitoring in the smart grid).

The spatial distribution of WNEs is neither completely random nor subject to planned installation [5]. Instead, most of the WNEs are typically clustered around certain points of interest, e.g., a collection of ZigBee sensors around a dual-mode Wi-Fi/ZigBee sink node, or a set of access points inside a building [6]. This spatial property is increasingly identified to characterize most of the current state-of-the-art networking systems and to play a key role to their statistical behavior [5]–[9]. Even though the clustered installation of WNEs is prominent in the present HWN, the relative distances and angles between the WNEs still govern the performance of all functions necessary for its fundamental operation, e.g., WNE discovery, association, and power control. In this direction, more and more radio access technologies (RATs) incorporate a suite of measurement capabilities to their baseline operation that enable WNEs of the same RAT to directly (or indirectly) estimate the relative distance or angle between them, e.g., Timing Difference (TD) [10], Angle of Arrival (AoA) [10], Time of Arrival (ToA) [11], Received Signal Strength (RSS) [2], [10], and Radio Frequency (RF) power level [3]. The employment of such measurements is the cornerstone of location estimation upon which a WNE estimates its relative position (distance, angle) with respect to another target WNE of the same RAT [12].

Location estimation is a key prerequisite for location-aware decision making [13]. Among others, it can significantly improve the performance of *proximity estimation* upon which a tagged WNE (*source WNE*) identifies its physical proximity (or connectivity) to another WNE (*target WNE*). When the two tagged WNEs support the same RAT, proximity estimation is typically referred to as peer discovery [14], [15]. Recently, there has been a surge of interest on proximity estimation between

D. Xenakis, L. Merakos, and N. Passas are with the Department of Informatics and Telecommunications, University of Athens, Athens 157 84, Greece (e-mail: nio@di.uoa.gr; merakos@di.uoa.gr; passas@di.uoa.gr).

M. Kountouris is with the Mathematical and Algorithmic Sciences Lab, France Research Center, Huawei Technologies Co. Ltd., Boulogne-Billancourt 92100, France (e-mail: marios.kountouris@huawei.com).

C. Verikoukis is with the Centre Tecnologic de Telecomunicacions de Catalunya, Barcelona 08860, Spain (e-mail: cveri@cttc.es).

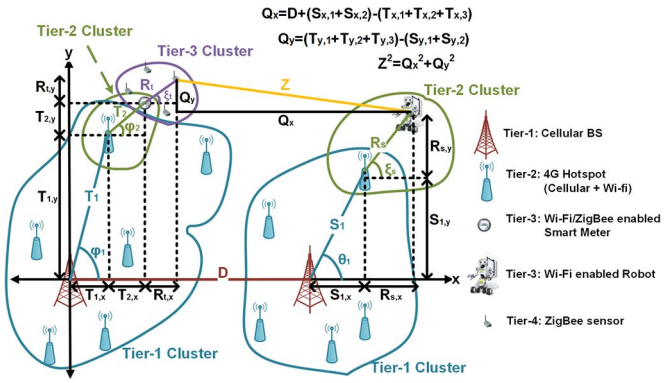

Fig. 1. Proximity estimation given spatial information from the heterogeneous WNEs.

WNEs that do not necessarily support (or associate with) the same RAT. Social networking, massive multiplayer online gaming, device-to-device communications, smart metering, first-responder communications, and unsupervised navigation of communication-aware robotic nodes are only a few of the emerging applications motivating this disruptive functionality [4], [17], [18]. Besides, proximity estimation is the inextricable prelude for the direct exchange of localized traffic between nearby WNEs, a.k.a. *machine-type communications* [19], [20], and a vital component of the future 5G network where the estimation of proximity between the myriads of WNEs can be a limiting performance factor [21].

Fig. 1 provides an illustrative example of a multi-tier clustered HWN. To better comprehend the benefits of proximity estimation between heterogeneous WNEs, let us consider that the dual-mode Wi-Fi/ZigBee robot (source WNE) seeks to discover a malfunctioning ZigBee sensor (target WNE) to replace it. The strategic integration of spatial information from (as many as possible) heterogeneous WNEs enables the robot to navigate towards the malfunctioning sensor, even when they are separated by a large geographical distance. Such an approach is (perhaps) the only viable solution to the problem since, on the one hand, the low-cost sensor is unable to employ GPS-assisted location estimation and, on the other hand, the frequent use of the energy-consuming GPS receiver at the (battery-operated) robot can rapidly deplete its battery.

In this work, we develop an analytical framework that aims at providing an answer to the relevant and interesting question of what is the probability that two tagged WNEs are in proximity, even if the respective nodes are not capable of communicating directly, e.g., large separation distance, or support of different RATs. To achieve this, we correlate the locations of the source and the target WNEs (and estimate their relative distance), by incorporating existing knowledge for their locations relative to their upper-tier WNEs in the HWN (up to tier-1). When such knowledge is not available, we employ stochastic modeling for estimating the location of a WNE relative to its upper-tier WNE(s). Although such an approach can be subject to erroneous positioning measurements or increased uncertainty (due to the modeling assumptions), it also enables proximity estimation between nodes separated by a large geographical distance or supporting different RATs. Besides, current literature includes a plethora of practical techniques for employing fine-grained location estimation and mitigating prominent effects of the wireless medium [11], [12], [18], [22].

In this direction, we propose an analytical framework that integrates existing knowledge of the actual HWN layout, e.g., clustering relations and relative position measurements, and employs stochastic modeling to assess the spatial relations that are not known for the HWN layout. To achieve this, we propose an M-tier model of networking clusters that captures the key spatial dependencies between the WNEs of the today's HWN. This model enables us to assess the performance of proximity estimation among two tagged (and not necessarily homogeneous) WNEs, given partial knowledge of the HWN layout. Under this model, we show that the probability that the two tagged WNEs are in proximity is given by the (conditional) cumulative distribution function (cdf) of their relative distance. Accordingly, we derive closed-form expressions on the distribution of the relative distance between the two WNEs, given partial knowledge of the relative distances and angles of their upper-tier WNEs. The derived expressions enable us to derive optimal strategies for the deployment of upper-tier WNEs, as means of maximizing the probability of proximity between WNEs that reside in lower-tiers. Numerical results conclude our work, providing valuable insights for the design of location-aware proximity estimation in HWNs.

A. Related Works

The Poisson point process (PPP) has been recently shown to be as accurate as the grid model and a good fit for modeling the locations of small-sized stations in multi-tier cellular networks with independent tiers [1]. Besides, the PPP model has been used to derive near-optimal strategies for random peer discovery in homogeneous networks [14] and quantify its performance under the joint impact of channel fading and random node distribution [15]. Nonetheless, more sophisticated point process (PP) models have been recently studied to capture the repulsiveness among macrocell base stations observed in real-world cellular networks [16]. In parallel, a considerable amount of works identify that the locations of short-range WNEs are not completely random, e.g., sensors [8], femtocells [9], hotspots [5], or more generic WNEs [6], [7], while they typically form clusters around other WNEs of higher radii. Different from the aforementioned works, in this paper we propose an M-tier HWN model that accounts for both the multi-tiered structure of the present HWN and the clustering of short-range WNEs around WNEs of higher radii. Under this model, we develop an analytical framework that enables flexible integration of existing knowledge for the HWN layout upon evaluating the probability that two tagged WNEs are in proximity. Also, different from [14], [15], we integrate existing knowledge of the HWN layout in the proximity estimation process, i.e., conditional distributions, and focus on the (more general) scenario where the two tagged WNEs are not (necessarily) capable of communicating directly, e.g., due to large separation distance or the support of different RATs.

Location estimation poses several challenges that span from mitigating (or exploiting) prominent effects of the wireless medium [11], [13], [18] to employing cooperative localization [12], [22]. The impact of non line-of-sight (NLOS) propagation on localization is discussed in [11], where the authors propose regression algorithms to robustly identify and mitigate it in the

ultra wide-band (UWB) network. The authors in [18], demonstrate how the spatial predictability of wireless channels can be exploited, to jointly optimize the communication and motion plan of robots over predefined trajectories. The performance of cooperative RF-based localization between homogeneous WNEs is assessed in [12]. The interplay between the accuracy and the communication delay upon cooperative localization is analyzed in [22], where it is shown that standard cooperation results in the worst possible accuracy/delay trade-off. It follows that current literature includes a noteworthy amount of studies/ techniques for handling prominent effects of the wireless medium and employing fine-grained location estimation in practical network deployments [11], [12], [18], [22]. Under this viewpoint, instead of analyzing the performance of proximity estimation in the presence of localization errors, in this work, we focus on integrating location information from different WNEs to enable proximity estimation between WNEs that are not necessarily capable of communicating directly. Besides, as shown in the numerical results section, the results of our analysis can be used to identify conditions under which the localization precision can be relaxed without significantly affecting the performance of proximity estimation. To the best of our knowledge, this is the first attempt to evaluate the performance of proximity estimation between non-homogeneous WNEs given partial (or full) knowledge of the HWN layout.

B. Key Contributions

The key contributions of our work are as follows:

- We develop an analytical framework that integrates existing knowledge from the ubiquitous HWN infrastructure and employs stochastic modeling, to enable proximity estimation between WNEs that are not necessarily capable of communicating directly. The proposed framework launches the design of innovative proximity services when network coverage is sparse or when GPS-based localization is unavailable, e.g., indoor buildings, industrial areas, mines, underground parking lots.
- We derive closed-form expressions for the conditional probability distribution of the distance Z between two (not necessarily homogeneous) WNEs, given partial knowledge of the spatial relations between their upper-tier parent WNEs.
- We analyze the performance of proximity estimation between (not necessarily homogeneous) WNEs given different levels of knowledge for the HWN layout.
- We derive optimal strategies for the placement of upper-tier WNEs as means of maximizing the probability that two WNEs of interest are in proximity.
- We provide valuable insights for the design of location-aware proximity estimation in HWNs. We show that a denser tier-1 layout may deteriorate the performance of proximity estimation. We also show that the accuracy of AoA measurements can be relaxed in the low-tier WNEs, without significantly affecting the performance of proximity estimation.

The remainder of this paper is organized as follows. In Section II, we present the proposed M-tier model, motivate our modeling assumptions, and outline the location information model. In Section III, we derive closed-form expressions for the distance distribution between two tagged WNEs, conditioned on different knowledge for the HWN topology. In Section IV, we present optimal strategies for the deployment of upper-tier WNEs, whereas in Section V, we investigate the impact of key system parameters on the performance of proximity estimation and draw useful guidelines for its design in the future HWN. Section VI includes our conclusions.

II. System Model

A. System Description

We consider a fairly general HWN of M tiers, where each tier consists of WNEs that serve similar communication purposes and support the same RAT. The WNEs belonging to the m-th tier are referred to as tier-m WNEs ($m = 1, \ldots, M$). We consider that the tier-1 WNEs form a homogeneous PPP Φ_1 with intensity λ in the Euclidean plane, e.g., medium to long range base stations, and that, for $m > 1$, the tier-m WNEs are clustered around *some of* the tier-$(m-1)$ WNEs. We emphasize on around *some of* and *not all* tier-$(m-1)$ WNEs, since in practical deployments we do not expect a tier-m cluster around every tier-$(m-1)$ WNE. Let Φ_m denote the complete PP of tier-m WNEs, i.e., the union of all tier-m clusters. Given that a tier-m cluster is present around the tier-$(m-1)$ WNE $v_i \in \Phi_{(m-1)}$, we assume it to be in the form $N_{v_i}^m = N_i^m + v_i$, where the point sets N_i^m are independently and identically distributed (i.i.d) and independent of the parent PP Φ_{m-1}. All tier-m clusters ($m > 1$) are modeled by the Thomas cluster process (ThCP) as follows [6]: a) the number of points in each tier-m cluster is Poisson distributed with mean $\bar{c}_m$, and b) the WNEs in a tier-m cluster are scattered independently according to a symmetric normal distribution around the parent tier-$(m-1)$ WNE with variance σ_m^2.

We now turn our attention to two tagged WNEs, coined as the *source* and the *target* WNEs. We consider that the source WNE associates with a tier-m_s WNE, coined as the *associated WNE of the source WNE*, and that the target WNE associates with a tier-m_t WNE, coined as the *associated WNE of the target WNE*. The associated WNEs of the source/target WNEs can belong to different tiers in the HWN and support different RATs. Moreover, the source and the target WNEs are not necessarily part of the HWN infrastructure. Consider for example the spatial distribution of Wi-Fi users around a Wi-Fi hotspot as compared to that of Wi-Fi sensors around a Wi-Fi sink node (aggregation point). Even though both the Wi-Fi users and the Wi-Fi sensors are clustered around a WNE of the same tier, different properties characterize the spatial distribution of the end terminals (Wi-Fi users) and the low-tier network infrastructure (sensors). For this reason, we choose to model the locations of the source and the target WNEs (relative to their associated WNEs) explicitly. In particular, we consider that the source and the target WNEs are scattered indepedently around their associated WNEs according to the ThCP as well, with deployment variances σ_s^2 and σ_t^2, respectively.

Assumption 1: Let (x_u, y_u) and (x_v, y_v) denote the Cartesian coordinates of a tier-m WNE $u \in N_v^m$ and its parent tier-$(m-1)$ WNE $v \in \Phi_{m-1}$, respectively. The x and y components of the relative distance between the tier-m WNE u and its parent tier-$(m-1)$ WNE v, i.e., the random variables $x_m = x_u - x_v$ and $y_m = y_u - y_v$, are independent.

Assumption 1 states that the knowledge of the relative x-axis distance between a WNE and its parent WNE does not provide any information on the relative distance in the y-axis. We consider the same assumption to hold for the x and y components of the relative distance between the source/target WNEs and their associated WNEs. Lemma 1 readily follows from Assumption 1.

Lemma 1: The x and y components of the relative distance between a tier-m WNE u and its parent tier-$(m-1)$ WNE v, i.e., the random variables $x_m = x_u - x_v$ and $y_m = y_u - y_v$, are independent and normally distributed with variance σ_m^2.

Proof: Can be readily proved by using Assumption 1 and the methodology in [26]. □

If not fixed and known, the distance D between a tier-1 WNE and its k-th nearest WNE in Φ_1 follows a generalized Gamma distribution (k is termed as their neighboring degree).

Lemma 2: The pdf $f_D(d)$ of the distance D between a tier-1 WNE and its k-th nearest neighbor in Φ_1 is given by

$$f_D(d) = \frac{2(\pi\lambda)^k}{\Gamma[k]} d^{2k-1} e^{-\pi\lambda d^2}, \quad (1)$$

where $\Gamma[k]$ is the Gamma function.

Proof: The proof can be found in [23]. □

B. Location Information Model and Parameters

Since we are interested on analyzing how different levels of location-awareness affect the performance of proximity estimation in HWNs, we assume the presence of a location information server (LIS) that maintains fundamental knowledge of the HWN layout. In particular, we consider that the LIS is aware of the tier-1 intensity λ and the deployment variances σ_m^2 $(m > 1)$, σ_s^2 and σ_t^2. Besides, these parameters can be estimated by overhearing the pilot signals in the HWN, or by taking into account the typical range of different RATs, e.g., femtocells cover up to a few meters and UWB sensors up to a few centimeters. We further consider that part of the WNEs in the HWN can push/pull positioning measurements to the LIS over the common IP layer.

We assume that the LIS is aware of the clustering relations between the WNEs and capable of identifying the parent WNEs of the source/target WNEs up to tier-1. For brevity, we refer to the tier-m WNE in the sequence of parent WNEs for the source WNE as the *tier-m parent of the source WNE* ($m < m_s$), and use a similar terminology for the parents of the target WNE ($m < m_t$). In practice, the sequence of parent WNEs can be identified by exploiting knowledge from the installation phase, or by performing measurements on the TD, ToA, RSS, or RF power level, of higher-tier WNEs [2], [3], [10], [11]. For example, a dual-mode cellular/Wi-fi hotspot can measure the RSS from all nearby macrocells and set the one with the strongest signal as its parent. On the other hand, a sensor node can identify the nearest multi-RAT sink node by measuring the RF power level, or counting the number of hops to, all nearby sink nodes [3].

Aiming to capture the different levels of location-awareness that the LIS can provide to the two tagged WNEs, we consider it capable of utilizing spatial information on the relative distance and angle between two WNEs of interest. In Table I, we list the spatial information considered in this paper and provide insights on how it can be estimated in existing systems. Note that all angles are assumed to be measured with respect to the same reference direction: from the tier-1 parent of the target WNE to the tier-1 parent of the source WNE (Fig. 1). Nonetheless, in most of the 3GPP and IEEE-based systems, the WNEs perform angle measurements with respect to the (true) North [2], [10]. To resolve this issue, the LIS can utilize an additional measurement on the angle between the tier-1 parents (with respect to the true North) and subtract it from all angle measurements provided by the low-tier WNEs. In this fashion, all angles can be readily translated with respect to the desired reference direction (Fig. 1).

It is critical to note that we do not assume that the LIS has full knowledge of these measurements. Instead, we investigate how certain combinations of them affect the performance of proximity estimation in a HWN. The combined distance and angle measurements with respect to a target WNE can be viewed as the *relative polar coordinates* of the measuring WNE

TABLE I
LOCATION INFORMATION PARAMETERS (SPATIAL INFORMATION)

Parameter	Notation	Comments
Inter-site distance between the tier-1 parent WNEs of the tagged WNEs	D	Can be estimated by performing TD or Reference Signal Received Power (RSRP) measurements between the tier-1 parent WNEs of the WNEs [10].
Neighboring degree between the tier-1 parent WNEs of the WNEs	k	Can be estimated in a similar manner with D (lower accuracy is required).
Distance between the source WNE and its associated WNE	R_s	Can be estimated by performing TD [10], ToA [11], RSS [2], [10], or RF power level [3], either at the source WNE or its associated WNE.
Angle between the source WNE and its associated WNE	ξ_s	Can be estimated by performing AoA measurements [10] or by employing other indirect estimation methodologies depending on the RAT [25].ξ_s is measured with respect to the reference direction from the tier-1 parent of the target WNE to the tier-1 parent of the source WNE (Fig. 1).
Distance between the target WNE and its associated WNE	R_t	Can be estimated in a similar manner with R_s.
Angle between the target WNE and its associated WNE	ξ_t	Can be estimated in a similar manner with ξ_s. Measured with respect to the same reference direction with ξ_s.
Distance between the tier-*m* and the tier-*(m-1)* parent WNEs of the source WNE	S_{m-1}	Can be estimated by performing TD [10], ToA [11], RSS [2], [10], or RF power level [3], either at the tier-*m* parent WNE or at the tier-*(m-1)* parent WNE, depending on the RAT.
Angle between the tier-*m* and the tier-*(m-1)* parent WNEs of the source WNE	θ_{m-1}	Can be estimated in a similar manner with ξ_s, depending on the RAT. Measured with respect to the same reference direction with ξ_s.
Distance between the tier-*m* and the tier-*(m-1)* parent WNEs of the target WNE	T_{m-1}	Can be estimated in a similar manner with S_{m-1}.
Angle between the tier-*m* and the tier-*(m-1)* parent WNEs of the target WNE	ϕ_{m-1}	Can be estimated in a similar manner with ξ_s, depending on the RAT. Measured with respect to the same reference direction with ξ_s.

with respect to the target WNE. In the sequel, we denote by $\mathcal{L}_s$ and $\mathcal{L}_t$ the set of parent WNEs of the source and target WNE, respectively, for which the LIS has knowledge of their relative polar coordinates with respect to their upper-tier parent WNEs. The rest of the parent WNEs are denoted by $\bar{\mathcal{L}}_s$ and $\bar{\mathcal{L}}_t$, respectively. Fig. 1 depicts all parameters and random variables (RVs) involved in our analysis.

C. Performance Metrics

The performance of proximity estimation is tightly coupled with the definition of proximity between the WNEs. Aiming to cover both *range-based* and *connectivity-based* approaches [12], we define the *probability of probability* (PoP) as follows:

$$\mathcal{A}_{\mathcal{J}} \triangleq P\left[Z \leq \left(\frac{c}{Z_{th}} \right)^{\frac{1}{a}} \middle| \, \mathcal{J} \right], \tag{2}$$

where $\mathcal{J}$ denotes the available knowledge of the HWN topology, c is a scaling factor, a is a decay exponent, Z is the distance between the two tagged WNEs, and Z_{th} is a fixed threshold that guarantees proximity between the WNEs. Assuming that c refers to the transmit power at the source WNE (in Watts), a to the path loss exponent, and Z_{th} the receiver sensitivity at the target WNE (in Watts), (2) models the connectivity-based approach, i.e., $\mathcal{A}_{\mathcal{J}} = P[cZ^{-a} \geq Z_{th}|\mathcal{J}]$. In the contrary, for $c = 1$ and $a = -1$, (2) reduces to the range-based approach, i.e., $\mathcal{A}_{\mathcal{J}} = P[Z \leq Z_{th}|\mathcal{J}]$. From (2), it follows that the PoP is given by the cdf of the distance Z at the point $\left(\frac{c}{Z_{th}}\right)^{\frac{1}{a}}$, conditioned on the available knowledge $\mathcal{J}$. Note that in (2) we do not account for the impact of network interference. The main reason is that we focus on proximity estimation between WNEs that are not necessarily capable of communicating directly, i.e., the two WNEs can support different RATs.

D. Discussion on the System Model

In this section, we motivate our modeling assumptions and discuss their role in the subsequent analysis. Even though the PPP model has been extensively used to study the impact of the spatial distribution of macrocells on network performance, current literature includes PP models that better capture the spatial properties of macro-cellular networks, e.g., Determinental Point Processes (DPP) [5], [16]. In parallel, the authors in [25] have recently shown that existing results under the PPP model, can be generalized under other motion-invariant PP models as well, based on the Asymptotic Deployment Gain concept. In our work, we derive the distribution of the distance Z between two tagged WNEs, given location information including either the inter-site distance D or the neighboring degree k between their tier-1 parents.

Notably, the derived expressions given knowledge of the distance D apply under any motion-invariant PP model for tier-1. This can be readily shown if we consider that the probability distribution of the distance Z is conditioned on a *fixed* value of the distance D. In the contrary, the expressions given knowledge of the neighboring degree k require the probability distribution of the distance to the k-th nearest neighbor in tier-1. To the best of our knowledge, the distance distribution to the k-th nearest neighbor is available for only a few PP models, if not only the PPP model. Hence, even though more general models can be used to model the spatial distribution of tier-1 WNEs, the PPP model is the only tractable model for assessing the probability distribution of the distance Z given knowledge of the neighboring degree k. Accordingly, all subsequent derivations given knowledge of the neighboring degree k are limited to the PPP model for tier-1, leaving as future work potential extensions to more general spatial models for tier-1.

Let us now motivate our modeling assumptions on the spatial distribution of low-tier WNEs. In real-life HWNs, the deployment of short-range WNEs is purpose-driven and strongly depends on the geographical/demographic data. For example, hotspots are typically clustered around medium-sized base stations in a down-town region. Moreover, in sensor networks, sink nodes are installed close to the center-of-mass of lower-tier sensors, so as to aggregate traffic from as many as possible sensors and reduce deployment/operational costs. In the same direction, the authors in [5] conclude that, compared to other PP models, the class of poisson cluster processes (PCPs) better captures the key spatial depedencies in sensor networks, military platoons, and urban networks with dense hotspots. Besides, the ThCP belongs to the class of PCPs that have been extensively used to model the spatial distribution of sensors [8], femtocells [9], hotspots [5], and generic WNEs [6], [7], around their upper-tier WNEs. Notably, the ThCP model is also a good fit for the spatial distribution of remote radio units (RRU) around centralized processing units (CPUs), a.k.a. base-band pool, in the cloud—radio access network (C-RAN) architecture. In light of the above discussion, we consider that the ThCP model holds some important statistical properties that make it analytically tractable and practical. Besides, the proposed multi-tier model of ThCP-distributed clusters enables us to model the locations of the myriads of WNEs belonging to different RATs under a common analytical framework.

To better reveal the key parameters governing the proposed M-tier HWN model, in Fig. 2 we provide an illustrative example of a three-tier HWN that is in line with our system model. Note that, as discussed in Section III-A, the proposed M-tier model does not dictate the presence of a tier-m cluster around every tier-$(m-1)$ WNE. On the other hand, the ThCP model enables flexible modeling of the low-tier clusters by allowing different cluster populations (c_m) and deployment variances σ_m per networking tier ($m < M$). For example, the clustering relations are more prominent in the HWN of Fig. 2(a), i.e., $\sigma_1 = 200$ m^2 and $\sigma_1 = 30$ m^2, as compared to the HWN of Fig. 2(b), i.e., $\sigma_1 = 250$ m^2 and $\sigma_1 = 30$ m^2. We recognize that the selection of an appropriate deployment variance σ_m for $m < M$ is critical in the proposed M-tier model. Nonetheless, current literature includes a plethora of well-studied techniques for fitting sample data to symmetrical normal distributions (such as the one assumed under the ThCP model), e.g., method of moments, or maximum likelihood distribution fitting. Besides, the σ_m parameter refers to the entire HWN tier and can be estimated by averaging over meaningful realizations of the point process, or by utilizing existing reference subsets in the broader area of interest. Under this viewpoint, in the sequel we consider that, given the sample data/knowledge discussed in Section III-B, the LIS can employ existing distribution fitting techniques to estimate the deployment variance parameters per tier.

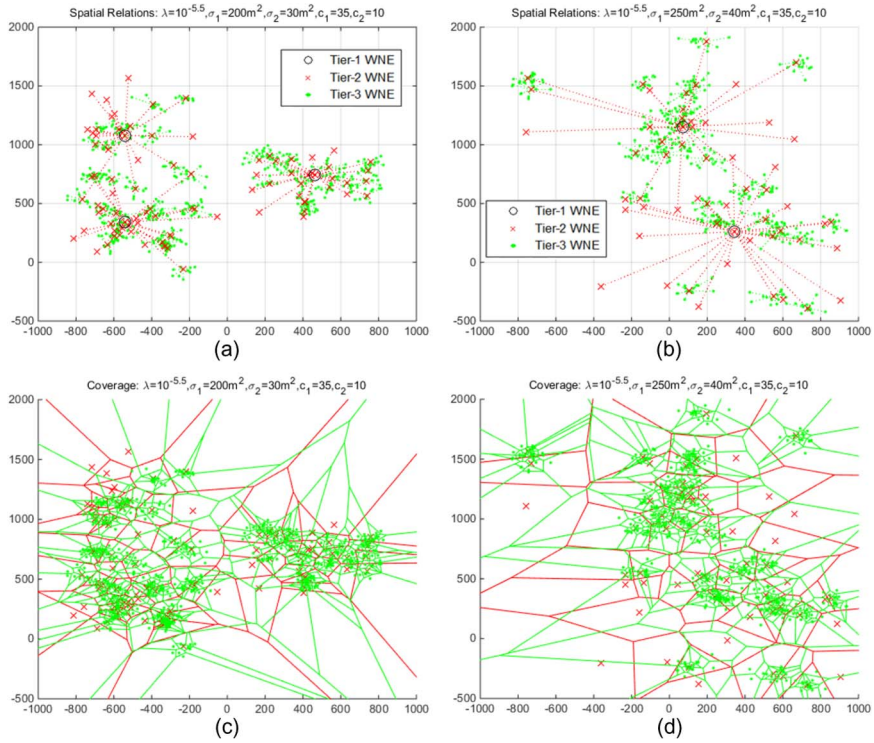

Fig. 2. Spatial relations and nearest-neighbor coverage in the proposed M-tier model.

Interestingly, the subsequent analysis can be readily extended to the case where the (known) distances/angles measurements are subject to random Gaussian noise. This follows from the fact that the locations of WNEs with unknown polar coordinates (relative to their parent WNEs) are modeled as Gaussian noise with known variance (ThCP model). Hence, an error analysis would be equivalent to the introduction of additional tier(s) with known variance.

III. Distance Distributions and Proximity Estimation in Multi-Tier HWNs

In Section III-A, we derive the pdf and the complementary cdf (ccdf) of the distance Z between two tagged WNEs, given knowledge of the distance D between their tier-1 parents and partial knowledge of the relative polar coordinates of the source/target WNEs (with respect to their associated WNEs), or the relative polar coordinates of *some* of their tier-m parent WNEs (with respect to their upper-tier parent WNEs). In Section III-B, we generalize the derived expressions to the case where, instead of the distance D, the LIS has knowledge of the neighboring degree k between the tier-1 parent WNEs. These expressions are of high practical interest as well, as they enable proximity estimation even if the LIS has imperfect knowledge of the distance D. Such a scenario can take place when the tier-1 WNEs face difficulties in accurately estimating their inter-site distance, e.g., indoor or unplanned deployment. In such occassions, the tier-1 WNEs can measure the RSS from other tier-1 WNEs and inform the LIS. Accordingly, the LIS can identify their neighboring degree by sorting the measurements in descending order. Such an approach, surpasses the need for accurate mapping between the RSS measurements and the distance D. Besides, the identification of k is less vulnerable to the effects of the wireless medium.

A. Distance Distribution Between Two WNEs Given at Least the Inter-Site Distance D

Theorem 1: The conditional pdf $f_{Z|D}(z)$ of the distance Z between the source and the target WNEs in a multi-tier clustered random HWN, given a) the distance D between their tier-1 parent WNEs and b) the relative polar coordinates of their parent WNEs in $\mathcal{L}_s$ and $\mathcal{L}_t$, is given by

$$f_{Z|D}(z) = \frac{z}{\sigma^2} e^{-\frac{\eta_x^2+\eta_y^2+z^2}{2\sigma^2}} I_0\left[\frac{z\sqrt{\eta_x^2+\eta_y^2}}{\sigma^2}\right], \tag{3}$$

where $I_0[x]$ is the modified Bessel function and the parameters η_x, η_y, and σ are given by:

$$\eta_x = D + \sum_{j\in\mathcal{L}_s} S_j \cos\phi_j - \sum_{i\in\mathcal{L}_t} T_i \cos\theta_i, \tag{4}$$

$$\eta_y = \sum_{i\in\mathcal{L}_t} T_i \sin\theta_i - \sum_{j\in\mathcal{L}_s} S_j \sin\phi_j, \tag{5}$$

$$\sigma^2 = \sum_{j\in\bar{\mathcal{L}}_s} \sigma_j^2 + \sigma_s^2 + \sum_{i\in\bar{\mathcal{L}}_t} \sigma_i^2 + \sigma_t^2. \tag{6}$$

The corresponding ccdf $\bar{F}_{Z|D}(z)$ is given by

$$\bar{F}_{Z|D}(z) = Q_1\left[\frac{\sqrt{\eta_x^2+\eta_y^2}}{\sigma}, \frac{z}{\sigma}\right], \tag{7}$$

where $Q_1[a,b]$ is the Marcum-Q function of the first order. If the relative polar coordinates (R_s, ξ_s) of the source WNE and/or (R_t, ξ_t) of the target WNE are also given, (3) and (7) hold with η_x, η_y, and σ, as given in Appendix A.

Proof: See Appendix A. □

Theorem 1 can be used to analytically evaluate the probability that two WNEs are in proximity, given any combination of spatial information that includes the distance D. The requirement of knowing D can be readily met in practical HWNs, where the locations of tier-1 WNEs typically remain fixed over time. The results in Theorem 1 not only allow heterogeneous WNEs to handle the uncertainty on their proximity, but also enable them to employ different levels of location-awareness upon proximity estimation depending on the available spatial information. Since different communication radii are met for the different WNEs of a HWN, more accurate estimates on the relative polar coordinates of low-tier WNEs will be critical only for applications requiring high proximity estimation accuracy, e.g., when a physical/visual contact is required. Note that Theorem 1 also applies when the tier-1 parent WNE of the two tagged WNEs is common, i.e., $D = 0$. Under the proposed HWN model of multi-tier ThCP-based clusters, Corollary 1 calculates the distance between two tagged WNEs when the LIS has full knowledge of the involved WNEs.

Corollary 1: The distance Z between the source and the target WNEs in a multi-tier clustered random HWN, given a) the distance D between their tier-1 parent WNEs, b) the relative polar coordinates (S_j, ϕ_j) of all parent WNEs of the source WNE ($1 < j \leq m_s$), c) the relative polar coordinates (T_i, θ_i) of all parent WNEs of the target WNE ($1 < i \leq m_t$), d) the relative polar coordinates (R_s, ξ_s) of the source WNE, and e) the relative polar coordinates (R_t, ξ_t) of the target WNE, is given by $Z = \sqrt{(D + Z_x)^2 + Z_y^2}$ where the parameters Z_x and Z_y are given by:

$$Z_x = \sum_{j=1}^{m_s} S_j \cos\phi_j + R_s \cos\xi_s - \sum_{i=1}^{m_t} T_i \cos\theta_i - R_t \cos\xi_t, \quad (8)$$

$$Z_y = \sum_{i=1}^{m_t} T_i \sin\theta_i + R_t \sin\xi_t - \sum_{j=1}^{m_s} S_j \cos\phi_j - R_s \sin\xi_s. \quad (9)$$

Proof: The proof is derived by plugging (20), (21), $R_{s,x} = R_s \cos\xi_s$, $R_{s,y} = R_s \sin\xi_s$, $R_{t,x} = R_t \cos\xi_t$ and $R_{t,y} = R_t \sin\xi_t$ in (17) (see Appendix A). □

B. Distance Distribution Between Two WNEs Given at Least the Neighboring Degree k

Let us now relax the requirement of having perfect knowledge of the distance D and extend our results to the scenario where the associated BSs can only identify k (more loose information).

Remark 1: The probability distribution of the distance Z, given the neighboring degree k between the tier-1 parent WNEs of the two tagged WNEs, is obtained by integrating out the distance $D \geq 0$ in the results of Theorem 1.

Note that the distance D is part of the η_x parameter in all scenarios in Theorem 1. Remark 1 can be used to numerically evaluate the distance distribution between the two WNEs of interest. In general, the integration of the Modified Bessel function in (3), or the Marcum-Q function in (7), with respect to D can not be expressed in closed-form. However, there exist two special cases where such integration gives closed-form expressions. The first case is when the LIS has knowledge of only the neighboring degree k, while the second case is when the LIS has knowledge of k and all parameters listed in Corollary 1 except from D. For brevity, in the second case we denote the respective pdf and ccdf by $f_{Z|k,full}(z)$ and $\bar{F}_{Z|k,full}(z)$, respectively.

Theorem 2: The conditional pdf $f_{Z|k}(z)$ of the distance Z between the source and the target WNEs in a multi-tier clustered random HWN, given only the neighboring degree k between their tier-1 parent WNEs, i.e., $L_s = \emptyset$ and $L_t = \emptyset$, is given by

$$f_{Z|k}(z) = \frac{1}{\sigma^2}\left(\frac{\epsilon_{k-1}-1}{\epsilon_{k-1}}\right)^k z e^{-\frac{\pi\lambda z^2}{\epsilon_{k-1}}} \cdot L_{k-1}\left[-\frac{\pi\lambda z^2}{(\epsilon_{k-1}-1)\epsilon_{k-1}}\right], \quad (10)$$

where $L_n[x]$ is the Laguerre polynomial and $\epsilon_{k-1} = 2\pi\lambda\sigma^2 + 1$. The ccdf $\bar{F}_{Z|k}(z)$ is given by

$$\bar{F}_{Z|k}(z) = \frac{e^{-\frac{\pi\lambda z^2}{\epsilon_{k-1}}}}{\epsilon_{k-1}} \sum_{n=0}^{k-1} \epsilon_n \left(\frac{\epsilon_{k-1}-1}{\epsilon_{k-1}}\right)^n \cdot L_n\left[-\frac{\pi\lambda z^2}{(\epsilon_{k-1}-1)(\epsilon_{k-1})}\right], \quad (11)$$

where $\epsilon_n = 1$ for all $n < k-1$.

Proof: See Appendix B. □

Theorem 3: The conditional pdf $f_{Z|k,full}(z)$ of the distance Z between the source and the target WNEs in a multi-tier clustered random HWN, given a) the neighboring degree k between their tier-1 parent WNEs, b) the relative polar coordinates (S_j, ϕ_j) of all parent WNEs of the source WNE ($1 < j \leq m_s$), c) the relative polar coordinates (T_i, θ_i) of all parent WNEs of the target WNE ($1 < i \leq m_t$), d) the relative polar coordinates (R_s, ξ_s) of the source WNE, and e) the relative polar coordinates (R_t, ξ_t) of the target WNE, is given by (12), shown at the bottom of the page, where $U[x]$ is the unit step function, $d_1 = -Z_x - \sqrt{z^2 - Z_y^2}$, $d_2 = -Z_x + \sqrt{z^2 - Z_y^2}$, and the parameters Z_x and Z_y are given by (8) and (9), respectively. The ccdf $\bar{F}_{Z|k,full}(z)$ is given by (13), shown at the bottom of the page, where $\Gamma[k, x]$ is the upper partial Gamma Function.

Proof: See Appendix C. □

IV. Optimal Network Deployment for Location-Aware Proximity Estimation

The strategic deployment of WNEs can play a key role in meeting purpose-driven targets. Consider for example the strategic deployment of sink nodes in industrial environments with numerous metering sensors. Even though the installation of additional sink nodes will enhance system robustness and improve network performance, e.g., decrease the number of multi-hop transmissions between the sensors, it will also increase network deployment costs and operational expenses. Hence, a key challenge is to identify the number of sink nodes that meet the capital/operational requirements set by the local operator while enabling effective proximity estimation among the sensor nodes deployed in a prescribed area. Another interesting example is the strategic placement of rapidly deployable cells and low-power sensors, as means of maximizing the probability of locating communication-enabled targets in emergency situations. A key challenge here is to adjust the

WNE density (or emission range) among the different tiers, given the available set of equipment, so as to maximize the probability that a communication-enabled target is identified to be in close proximity. Besides, maximizing the performance of proximity estimation between heterogeneous WNEs, e.g., an anchor point and a target device with unknown location, is of paramount importance in automated navigation systems, industrial installations, and underground facilities, e.g., mines, public transport platforms, parking buildings.

In light of the above discussion, in this section we derive useful guidelines on how to adjust the density (or range) of upper-tier WNEs, so as to maximize the capability of lower-tier WNEs to effectively estimate their physical proximity. Recall that, for a fixed area size, the deployment of additional tier-$(m-1)$ WNEs reduces the deployment variance in tier-m (σ_m^2). A reduced deployment variance σ_m^2 is also translated to shorter range for the tier-m WNEs. In the sequel, we identify the conditions under which the deployment variance σ^2 (Theorem 1) and the tier-1 intensity λ can maximize the probability of proximity between two tagged WNEs. When relevant, we derive approximate and exact expressions for the optimal σ^2 and λ parameters. Since in a real-world HWN not all tiers can be subject to optimization, we decompose the σ^2 parameter into two components: $\sigma^2 = \sigma_o^2 + \sigma_n^2$, where σ_o^2 refers to the sum of variances from tiers that are subject to optimization and σ_n^2 to the sum of the remaining variances that constitute σ^2.

Theorem 4: Let $\zeta = \sqrt{\eta_x^2+\eta_y^2}\left(\frac{c}{Z_{th}}\right)^{-\frac{1}{a}}$ and $\sigma^2 = \sigma_o^2 + \sigma_n^2$, where the parameters η_x, η_y, and σ^2 are as in Theorem 1. For $\zeta < 1$, the probability of proximity $\mathcal{A}_D$ decreases with σ_o^2. For $\zeta > 1$, the probability $\mathcal{A}_D$ attains an optimal operation point (maximum) if the sum of the variance(s) of interest, i.e., the σ_o^2 parameter, satisfies the following condition:

$$I_0\left[\frac{\eta_x^2+\eta_y^2}{\zeta\left(\sigma_n^2+\sigma_o^2\right)}\right] = \zeta I_1\left[\frac{\eta_x^2+\eta_y^2}{\zeta\left(\sigma_n^2+\sigma_o^2\right)}\right]. \tag{14}$$

The optimal variance, denoted by σ_o^{2*}, can be approximated by

$$\sigma_o^{2*} \approx \frac{8(\zeta-1)\left(\eta_x^2+\eta_y^2\right)}{\zeta(3\zeta+1)} - \sigma^2. \tag{15}$$

Proof: See Appendix D. □

Theorem 4 can be interpreted as follows. As the sum of the variances of interest (σ_o^2) decreases, the distance Z between the two WNEs tends to be probabilitistically closer to the known distance that separates the WNEs, i.e., the distance $\sqrt{\eta_x^2+\eta_y^2}$, which in turn, for $\zeta < 1$, is lower than the maximum range for successful proximity estimation, i.e., the parameter $\left(\frac{c}{Z_{th}}\right)^{-\frac{1}{a}}$. On the other hand, when $\zeta > 1$, the minimum (known) distance between the two WNEs is greater than the maximum range for successful proximity estimation. Thus, a higher uncertainty on the locations of the tagged WNEs and their parent WNEs, part of which are included in σ_o^2, increases the probability that the two WNEs are in proximity (up to a certain point: the value of σ_o^{2*}). We now turn our attention to the impact of the tier-1 intensity λ on the PoP $\mathcal{A}_{k,full}$. Notably, we show that when the LIS has knowledge of all parameters in Theorem 3, there exists an optimal tier-1 deployment strategy that maximizes the performance of location-aware proximity estimation.

Theorem 5: The probability of proximity $\mathcal{A}_{k,full}$: (a) is equal to 1 for $z \le |Z_y|$, (b) is equal to 0 for $z > |Z_y|$ and $d_2 \le 0$, (c) increases with λ for $z > |Z_y|$, $d_2 > 0$, and (d) exhibits an optimal operation point for $z > |Z_y|$, $d_2 > 0$, $d_1 > 0$, if the tier-1 intensity is given by

$$\lambda^* = \frac{k \ln \frac{d_1^2}{d_2^2}}{\pi\left(d_1^2 - d_2^2\right)}. \tag{16}$$

Proof: Properties (a) and (b) follow from (13). Property (c) follows from the fact that the derivative of $\mathcal{A}_{k,full} = 1 - \frac{\Gamma[k,\pi\lambda d_2^2]}{\Gamma[k]}$ with respect to λ, is always positive. Property (d) follows by differentiating $\mathcal{A}_{k,full} = \frac{\Gamma[k,\pi\lambda d_1^2]-\Gamma[k,\pi\lambda d_2^2]}{\Gamma[k]}$ with respect to λ and solving $\frac{\partial \mathcal{A}_{k,full}}{\partial \lambda} = 0$. □

V. Numerical Results and Design Guidelines

In this section, we analyze the impact of the key system parameters on the PoP given partial (or full) knowledge of the HWN topology. By using the results presented before, we identify how different levels of location-awareness affect the performance of proximity estimation and derive useful design guidelines for the today's HWN. When relevant, we consider the multi-tier HWN layout illustrated in Fig. 1.

A. On the Impact of the Deployment Variance σ^2 and the Tier-1 Intensity λ

In this section, we identify optimal strategies for the deployment of low-tier ($m > 1$) and tier-1 WNEs, and examine how partial knowledge of the HWN topology, or inaccurate positioning measurements, affect the performance of proximity estimation. In Fig. 3, we plot the impact of the standard deviation

$$f_{Z|k,full}(z) = \begin{cases} 0, & z \le |Z_y| \\ \frac{2(\pi\lambda)^k z}{\Gamma[k]\sqrt{z^2-Z_y^2}}\left(d_1^{2k-1}e^{-\pi\lambda d_1^2}U[d_1] + d_2^{2k-1}e^{-\pi\lambda d_2^2}U[d_2]\right), & z > |Z_y| \end{cases} \tag{12}$$

$$\bar{F}_{Z|k,full}(z) = \begin{cases} 0, & z \le |Z_y| \\ \frac{\left(\Gamma[k]-\Gamma\left[k,\pi\lambda d_1^2\right]\right)U[d_1]+\Gamma\left[k,\pi\lambda d_2^2\right]}{\Gamma[k]}, & z > |Z_y| \text{ and } d_2 > 0 \\ 1, & z > |Z_y| \text{ and } d_2 \le 0 \end{cases} \tag{13}$$

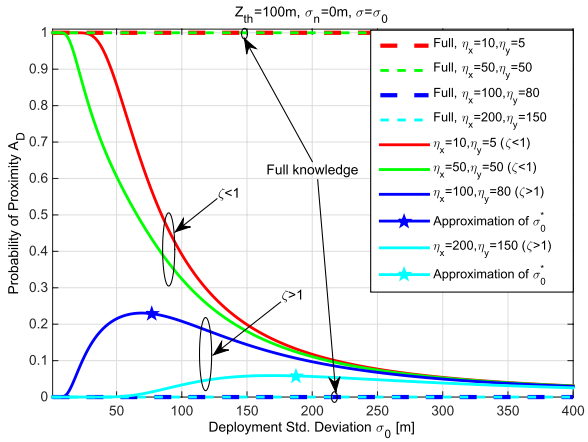

Fig. 3. Probability of Proximity given D vs. Deployment Std. Deviation σ.

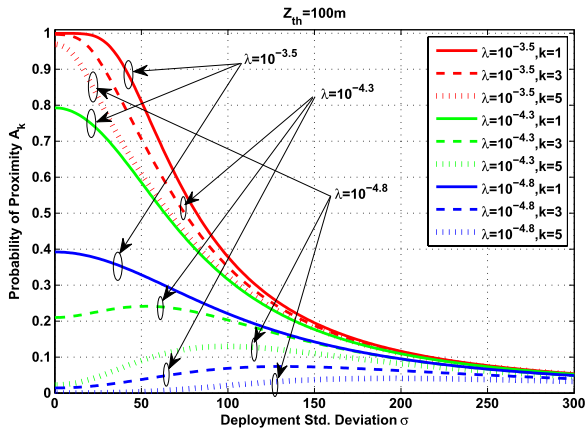

Fig. 4. Probability of Proximity given k vs. Deployment Std. Deviation σ.

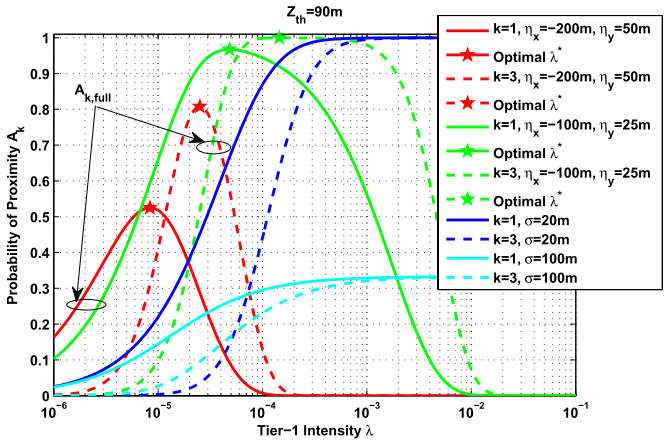

Fig. 5. Probability of Proximity given k vs. Tier-1 Intensity λ.

σ_0 on the PoP $\mathcal{A}_D$ (location information for at least the distance D). Recall that σ_0 is a measure of the uncertainty on the locations of WNEs around their parent WNEs, for which the LIS has no knowledge of their relative polar coordinates.

As expected, if the LIS has full knowledge on the coordinates of the source/ target WNEs and their parent WNEs, proximity estimation is either successful or not. Given $Z_{th} = 100$ m, $c = 1$, and $a = -1$, i.e., range-based discovery, the proximity estimation is successful ($\mathcal{A}_D = 1$) if the x-axis and y-axis components of the relative distance between the two WNEs, i.e., the η_x and η_y parameters, satisfy the condition $\eta_x^2 + \eta_y^2 \leq Z_{th}^2$, e.g., ($\eta_x = 10$ m, $\eta_y = 5$ m) and ($\eta_x = 50$ m, $\eta_y = 50$ m). Interestingly, when the LIS has partial (or inaccurate) knowledge of the parent WNEs coordinates, the behavior of $\mathcal{A}_D$ changes with σ_0 depending on the ratio of a) the known distance between the two tagged WNEs $\sqrt{\eta_x^2 + \eta_y^2}$, and b) the proximity threshold Z_{th}.

The aforementioned ratio corresponds to ζ in Theorem 4 (range-based discovery). For ($\eta_x = 10$ m, $\eta_y = 5$ m) and ($\eta_x = 50$ m, $\eta_y = 50$ m), which both result in $\zeta < 1$, the probability $\mathcal{A}_D$ decreases with σ_0. This behavior is in line with Theorem 4 and follows from the fact that a higher σ_0 prolongs the tail of the distance distribution between i) the WNEs with unknown relative polar coordinates and ii) their parent WNEs. Notably, σ_0 dominates the η_x and η_y parameters above a certain point, i.e., for $\sigma_0 > 200$ m $\mathcal{A}_D$ is roughly the same for all η_x and η_y values. On the other hand, for ($\eta_x = 100$ m, $\eta_y = 80$ m) and ($\eta_x = 200$ m, $\eta_y = 150$ m), which both result in $\zeta > 1$, the performance of proximity estimation improves with σ_0 up to a certain point. This behavior is due to the fact that for $\zeta > 1$, a small uncertainty on the coordinates of WNEs with unknown locations reduces the 'gap' between the known distance separating the two WNEs and the threshold Z_{th}. We note here that, the optimal σ_0^* in Fig. 3 is well approximated by the square root of (15) (highlighted with a star). The results in Fig. 3 highlight that the employment of more accurate positioning measurements is more meaningful when $\zeta < 1$, and that the deployment of additional low-tier WNEs should be carefully handled when $\zeta > 1$. These two design guidelines can be the basis for a) optimizing the frequency/accuracy of positioning at the WNEs so as to pertain the signaling/processing overhead at low levels and b) strategically deploying additional low tier WNEs to improve the performance of location-aware proximity estimation.

In Fig. 4 we plot the effect of σ on the PoP $\mathcal{A}_k$ for various values of k and λ. As expected, the probability $\mathcal{A}_k$ decreases with k. However, the impact of higher k is less evident when the WNEs are densely deployed, e.g., for $\lambda = 10^{-3.5}$ (one tier-1 WNE per 50 m^2), and becomes prominent in lower tier-1 intensities, e.g., for $\lambda = 10^{-4.8}$ (one tier-1 WNE per 250 m^2). Once again, σ is shown to dominate the performance of $\mathcal{A}_k$. Notably, Fig. 4 reveals the existence of optimal deployment strategies for the low-tier WNEs, even when the LIS is only aware of k, e.g., observe the curves for $k = 3, 5$ and $\lambda = 10^{-4.3}, 10^{-4.8}$. Besides, Fig. 4 highlights that even fundamental parameters on the HWN layout, such as the neighboring degree k, carry enough information to infer about the outcome of proximity estimation and optimize its performance. The results in Figs. 3 and 4 also indicate that the performance of proximity estimation remains roughly the same when the estimation process for the individual deployment variances involves an aggregate error of up to a few meters (for the proximity threshold under scope).

Let us now examine the impact of the tier-1 intensity on the PoP $\mathcal{A}_k$ (Fig. 5). When the LIS has knowledge of only the neighboring degree k, the probability $\mathcal{A}_k$ increases with λ and decreases with k (blue and cyan plots). This behavior is in line with intuition, since a higher λ reduces the mean inter-site distance between the tier-1 WNEs and a higher k increases it. However, the performance gains from the densification of tier-1 are limited by the uncertainty on the parent WNE locations (modeled by σ). For example, when the discovery threshold is

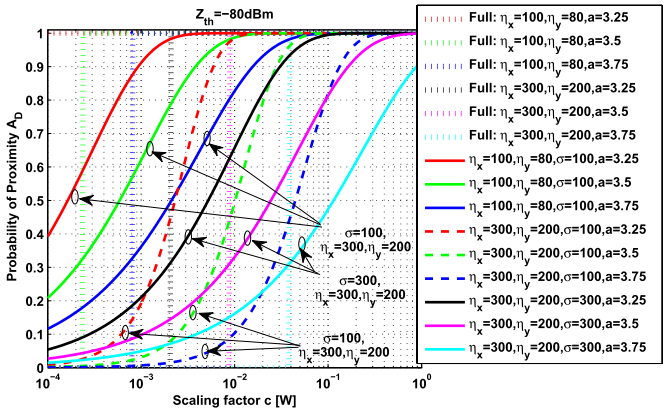

Fig. 6. Probability of Proximity given D vs. Scaling Factor c [W].

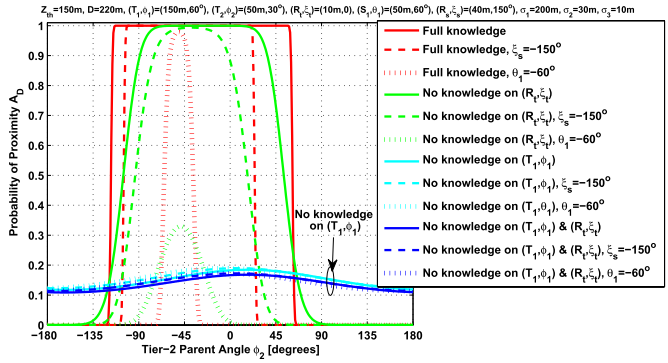

Fig. 7. Probability of Proximity given D vs. Tier-2 Parent Angle ϕ_2 [degrees].

lower than the aggregate std. deviation σ, e.g., $Z_{th} = 90$ m $< \sigma = 100$ m, an increase of the tier-1 intensity λ by two orders of magnitude leaves the performance of proximity estimation roughly unaffected (Fig. 5), e.g., for $\sigma = 100$ m and $\lambda = 10^{-3} \rightarrow 10^{-1}$. On the other hand, when the LIS is aware of k and has full knowledge of the relative polar coordinates of the tagged WNEs and their parent WNEs ($m > 1$), there exists an optimal tier-1 intensity λ^* that maximizes $\mathcal{A}_k$. This behavior is in line with Theorem 5 and, notably, the optimal tier-1 intensity λ^* is computed by (16) (highlighted with a star). When the tier-1 parent WNEs of the two tagged WNEs are distant neighbors, e.g., $k = 3$, the optimal λ^* shifts to higher values that statistically reduce the distance between the tier-1 WNEs. In addition, the performance gains from the densification of tier-1 are shown to be lower when the η_x and η_y components are high (green vs. red plots). Hence, if not subject to optimization, the deployment of additional tier-1 WNEs may deteriorate (rather than improve) the performance of proximity estimation when the LIS is aware of k (instead of D).

B. On the Impact of Transmit Power

We now turn our attention to the impact of the scaling factor c (connectivity-based discovery). The proximity threshold (receiver sensitivity) is set to $Z_{th} = -80$ dB. Given location information for at least the distance D, the PoP a) increases with the transmit power c, b) is inversely proportional to the path loss exponent a, and c) decreases with the relative distance components $|\eta_x|$ and $|\eta_y|$ (Fig. 6). When the LIS has full knowledge on the relative coordinates of the tagged WNEs and their parent WNEs (dotted lines), the transmit power c for successful proximity estimation can be readily estimated by using Corollary 1 (dotted lines). On the other hand, when the LIS has partial knowledge of the WNEs coordinates (solid and dashed lines), an increase of the distance components η_x and η_y is shown to be more preferable, in terms of transmit power requirements, compared to a similar increase to the uncertainty on the WNEs locations (modeled by σ). This relation can be easily observed by comparing the red solid, red dashed, and black solid lines. Thus, when the transmit power is a limiting performance factor at the source WNE, the utilization of measurements (to lower the uncertainty on the WNEs locations) can play a key role in reducing the power transmissions/consumption required for proximity estimation. An instantiation of such an approach, is the employment of measurements from the tier-1 and tier-2 parent WNEs of the ZigBee sensor (target WNE) in Fig. 1, as means of reducing the transmit power for proximity estimation at the battery-operated robot (source WNE).

C. On the Impact of Angles Between the WNEs

The employment of accurate AoA measurements increases the complexity and processing requirements for the radio transceiver. With this in mind, in Fig. 7 we investigate the impact of the ϕ_2 angle between the tier-3 and the tier-2 parents of the target WNE on the PoP $\mathcal{A}_D$. As expected, when the LIS has full knowledge on the locations of the tagged WNEs and their parent WNEs, proximity estimation can be either successful or not. Notably, there exists a ϕ_2 interval within which the PoP remains roughly unaffected. This interval is shown to be expanded, shifted, or compressed, in relation with the rest of the parameters governing the HWN topology. For example, if the angle ξ_t between the target WNE and its parent tier-3 WNE is equal to $-150°$ (instead of $150°$), then the ϕ_2 interval for successful proximity estimation is compressed and shifted to the left (red dashed line in Fig. 7). This effect is due the fact that for $\theta_2 = -150°$ the two tagged WNEs are separated by a higher distance (Fig. 1). Even more evident is the compression of the ϕ_2 interval when the angle between the tier-1 and tier-2 parent WNEs of the source WNE is set to $\theta_1 = -60°$ instead of $(\theta_1 = 60°)$ (red dotted line), since the distance between them is even higher. Such an effect is expected in the today's HWN, where the distance between upper-tier WNEs is higher compared to the one between lower-tier WNEs.

Interestingly, a similar interval exists when the LIS is not aware of the relative coordinates of the target WNE (green lines). Notice that the lack of such information prolongs the tail of the respective ϕ_2 interval with full knowledge in both directions. When the LIS has no knowledge of the coordinates (T_1, θ_1) of the tier-2 parent WNE, the probability $\mathcal{A}_D$ is shown to remain roughly unaffected by the values of ϕ_2 (blue and cyan lines). This relation indicates that the benefits from performing accurate measurements on the angles between low-tier WNEs is marginal when the relative coordinates of high-tier parent WNEs are not known to the LIS.

From the discussion above, we draw two important design guidelines. Firstly, the accurate estimation of the angle between low-tier WNEs and their parent WNEs is necessary only When accurate proximity estimation is required, e.g., the proximity

threshold Z_{th} is low. Secondly, depending on the available spatial information, the low-tier WNEs can relax the accuracy of AoA measurements without significantly deteriorating the performance of proximity estimation. The range of this relaxation (error tolerance) can be estimated by exploiting the results presented in this work.

VI. Conclusion

More and more WNEs are capable of estimating their distance and angle to other nearby WNEs of the same technology. Integrating such spatial information from the ubiquitous WNEs of different RATs is a key enabler for fine-grained proximity estimation. In this paper, we have analyzed how partial knowledge of the HWN topology affects the distance distribution between two not necessarily nearby or homogeneous WNEs. To achieve this, we have developed an analytical framework that is capable of correlating the locations of two tagged WNEs to estimate their relative distance. A key feature of the proposed framework is the incorporation of existing knowledge for the locations of the tagged WNEs relative to their upper-tier WNEs in combination with stochastic modeling when such knowledge is not available. Even though the use of cluster models typically involves numerical integration, we have shown that the proposed multi-tier ThCP-based HWN model enables the derivation of closed-form expressions on the performance of proximity estimation. Among others, we have shown that even basic information on the HWN layout carries enough information for estimating the outcome of proximity estimation and fine-tuning its performance. Also, we have identified conditions under which the strategic installation of WNEs, or the use of positioning measurements from other WNEs, enhance the performance of location-aware proximity estimation. Finally, we have shown that, depending on the availability of spatial information, the low-tier WNEs can relax the accuracy of AoA measurements while pertaining a PoP target.

Appendix

A. Proof of Theorem 1

Let $T_{i,x}$ and $T_{i,y}$ denote the x and y-axis components (projections), respectively, of the *relative* distance between the tier-i and tier-$(i-1)$ parent WNEs of the target WNE as shown in Fig. 1 ($i \leq m_t$). In addition, let $S_{j,x}$ and $S_{j,y}$ denote the respective x and y-axis components of the *relative* distance between the tier-j and tier-$(j-1)$ parent WNEs of the source WNE ($j \leq m_s$). Then, the distance Z between the two tagged WNE is given by (17), shown at the bottom of the page.

For $i \in \mathcal{L}_t$, where $\mathcal{L}_t$ is the set of parent WNEs of the target WNE for which the relative polar coordinates are known, the x and y-axis components of the relative distance T_i between the tier-i and the tier-$(i-1)$ parent WNEs of the target WNE can be readily computed by

$$T_{i,x} = T_i \cos\theta_i \text{ and } T_{i,y} = T_i \sin\theta_i, \text{ for } i \in \mathcal{L}_t. \quad (20)$$

Similarly, for $j \in \mathcal{L}_s$, where $\mathcal{L}_s$ is the set of parent WNEs of the source WNE for which the relative polar coordinates are known, the x and y-axis components of the relative distance S_j between the tier-j and the tier-$(j-1)$ parent WNEs of the source WNE are given by

$$S_{j,x} = S_j \cos\phi_j \text{ and } S_{j,y} = S_j \sin\phi_j, \text{ for } j \in \mathcal{L}_s \quad (21)$$

If the relative polar coordinates (R_t, ξ_t) of the target WNE are known to the LIS, then the x and y-axis components of the distance R_t between the target WNE and its associated WNE are given by $R_{t,x} = R_t \cos\xi_t$ and $R_{t,y} = R_t \sin\xi_t$, respectively. On the other hand, if the relative polar coordinates (R_s, ξ_s) of the source WNE are known, then the x and y-axis components of the distance R_s between the source WNE and its associated WNE are given by $R_{s,x} = R_s \cos\xi_s$ and $R_{s,y} = R_s \sin\xi_s$, respectively. Let us now define two RVs Q_x and Q_y as in (18) and (19), shown at the bottom of the page.

By combining (17)–(19) it can be readily shown that $Z = \sqrt{Q_x^2 + Q_y^2}$. Let us assume that the relative polar coordinates of the source and target WNEs are not known to the LIS. By taking a closer look to (18) it can be seen that the RV Q_x is composed by i) a sum of fixed and known parameters, i.e., the sum $(D + \sum_{j\in\mathcal{L}_s} S_j \cos\phi_j - \sum_{i\in\mathcal{L}_t} T_i \cos\theta_i)$, and ii) a sum of unknown RVs, i.e., the sum $(\sum_{j\in\tilde{\mathcal{L}}_s} S_{j,x} + R_{s,x} - \sum_{i\in\tilde{\mathcal{L}}_t} T_{i,x} - R_{t,x})$. From Lemma 1, the x component of the relative distances T_i and S_j, i.e., the RVs $T_{i,x}$ and $S_{j,x}$, are normally distributed with variance σ_i^2 and σ_j^2, respectively. Under the assumption of independence of the x and y distance components between the source/target WNEs and their associated WNEs (Section II), it can be proved that the RVs $R_{s,x}$ and $R_{t,x}$ are normally distributed with variance σ_s^2 and σ_t^2, respectively. Note that this property is an artefact of the proposed HWN model that consists of multi-tier ThCP-based clusters.

On the other hand, the RVs $T_{i,x}$, $S_{j,x}$, $R_{s,x}$ and $R_{t,x}$ are mutually independent. The independence follows by construction, since i) all tier-m clusters are i.i.d. and independent of the parent tier-$(m-1)$ PP Φ_{m-1}, and ii) the locations of the two tagged WNEs are mutually independent and independent from the locations of other WNEs (Section II). Now, since the RV Q_x is composed by a fixed sum and a sum of mutually independent and normally distributed RVs (18), it can be proved that it is normally distributed with mean $\eta_x = (D + \sum_{j\in\mathcal{L}_s} S_j \cos\phi_j - \sum_{i\in\mathcal{L}_t} T_i \cos\theta_i)$ and variance $\sigma^2 = (\sum_{j\in\tilde{\mathcal{L}}_s} \sigma_j^2 + \sigma_s^2 + \sum_{i\in\tilde{\mathcal{L}}_t} \sigma_i^2 + \sigma_t^2)$, i.e., $Q_x \sim \mathcal{N}(\eta_x, \sigma^2)$.

By following a similar approach, it can be shown that Q_y is normally distributed with mean $\eta_y = (\sum_{i\in\mathcal{L}_t} T_i \sin\theta_i - \sum_{j\in\mathcal{L}_s} S_j \sin\phi_j)$ and variance σ^2. Furthermore, Q_y and Q_x are independent, since all RVs that constitute Q_y (y-axis components) are independent of the ones that constitute Q_x (x-axis components). The independence follows by Lemma 1 and by using the facts that i) the x and y components of the relative distance between the source/target WNEs and their associated WNEs are independent, ii) all tier-m clusters are i.i.d. and independent of the parent tier-$(m-1)$ PP Φ_{m-1}, and iii) the locations of the two tagged WNEs are mutually independent and independent of the locations of other WNEs (Section II). Since the RVs $Q_x \sim \mathcal{N}(\eta_x, \sigma^2)$ and $Q_y \sim \mathcal{N}(\eta_y, \sigma^2)$ are independent, their joint density is given by

$$f_{Q_x,Q_y}(x, y) = \frac{1}{2\pi\sigma^2} e^{-\frac{(x-\eta_x)^2+(y-\eta_y)^2}{2\sigma^2}}. \quad (22)$$

Now, let ΔA_z denote the region of the plane such that $z < \sqrt{x^2+y^2} < z + \mathrm{d}z$. Then, the region ΔA_z is a circular ring with inner radius z and thickness $\mathrm{d}z$ [27]. By working in polar coordinates, i.e., $x = z\cos\xi$, $y = z\sin\xi$, and $\mathrm{d}x\mathrm{d}y = z\mathrm{d}z\mathrm{d}\xi$, we get

$$f_{Z|D}(z)\mathrm{d}z = \int_{\Delta A_z} f_{Q_x,Q_y}(x,y)\mathrm{d}x\mathrm{d}y \tag{23}$$

$$= \frac{1}{2\pi\sigma^2}\int_0^{2\pi} e^{-\frac{(z\cos\xi-\eta_x)^2+(z\sin\xi-\eta_y)^2}{2\sigma^2}} z\mathrm{d}z\mathrm{d}\xi. \tag{24}$$

By eliminating $\mathrm{d}z$ from both sides in (24) and solving the integral, we finally reach (3). We now derive the conditional ccdf $\bar{F}_{Z|D}(z)$ as follows:

$$\bar{F}_{Z|D}(z) = \int_z^\infty f_{Z|D}(x)\mathrm{d}x \tag{25}$$

$$= \int_z^\infty \frac{x}{\sigma^2} e^{-\frac{\eta_x^2+\eta_y^2+x^2}{2\sigma^2}} I_0\left[\frac{x\sqrt{\eta_x^2+\eta_y^2}}{\sigma^2}\right]\mathrm{d}x \tag{26}$$

$$= Q_1\left[\frac{\sqrt{\eta_x^2+\eta_y^2}}{\sigma}, \frac{z}{\sigma}\right], \tag{27}$$

where $Q_M[a,b]$ is the Marcum-Q function [28], (25) is derived by substituting (3), and (27) by the definition of the Marcum-Q function, i.e., $Q_M[a,b] = \int_b^\infty x\left(\frac{x}{a}\right)^{M-1} e^{-\frac{x^2+a^2}{2}} I_{M-1}[ax]\mathrm{d}x$, where $I_{M-1}[x]$ is the modified Bessel function of the first kind and $(M-1)$-th order. Using a similar methodology, it can be shown that (3), (27) also apply when the LIS has additional knowledge of the relative polar coordinates of the source WNE and/or the target WNE. However, the parameters η_x, η_y, and σ^2 should be replaced as follows. If the relative polar coordinates (R_s, ξ_s) of the source WNE are available, then

$$\eta_x = D + \sum_{j\in\mathcal{L}_s} S_j\cos\phi_j + R_s\cos\xi_s - \sum_{i\in\mathcal{L}_t} T_i\cos\theta_i, \tag{28}$$

$$\eta_y = \sum_{i\in\mathcal{L}_t} T_i\sin\theta_i - \sum_{j\in\mathcal{L}_s} S_j\sin\phi_j - R_s\sin\xi_s, \tag{29}$$

$$\sigma^2 = \sum_{j\in\bar{\mathcal{L}}_s}\sigma_j^2 + \sum_{i\in\bar{\mathcal{L}}_t}\sigma_i^2 + \sigma_t^2. \tag{30}$$

If the relative polar coordinates (R_t, ξ_t) of the target WNE are available, then

$$\eta_x = D + \sum_{j\in\mathcal{L}_s} S_j\cos\phi_j - \sum_{i\in\mathcal{L}_t} T_i\cos\theta_i - R_t\cos\xi_t, \tag{31}$$

$$\eta_y = \sum_{i\in\mathcal{L}_t} T_i\sin\theta_i + R_t\sin\xi_t - \sum_{j\in\mathcal{L}_s} S_j\sin\phi_j, \tag{32}$$

$$\sigma^2 = \sum_{j\in\bar{\mathcal{L}}_s}\sigma_j^2 + \sigma_s^2 + \sum_{i\in\bar{\mathcal{L}}_t}\sigma_i^2. \tag{33}$$

If the relative polar coordinates of both the source and the target WNEs are available, then

$$\eta_x = D + \sum_{j\in\mathcal{L}_s} S_j\cos\phi_j + R_s\cos\xi_s - \sum_{i\in\mathcal{L}_t} T_i\cos\theta_i - R_t\cos\xi_t, \tag{34}$$

$$\eta_y = \sum_{i\in\mathcal{L}_t} T_i\sin\theta_i + R_t\sin\xi_t - \sum_{j\in\mathcal{L}_s} S_j\sin\phi_j - R_s\sin\xi_s, \tag{35}$$

$$\sigma^2 = \sum_{j\in\bar{\mathcal{L}}_s}\sigma_j^2 + \sum_{i\in\bar{\mathcal{L}}_t}\sigma_i^2. \tag{36}$$

B. Proof of Theorem 2

Provided that $\mathcal{L}_s = \emptyset$ and $\mathcal{L}_t = \emptyset$, the parameters in (4)–(6) are given by $\eta_x = D$, $\eta_y = 0$, and

$$\sigma = \sum_{j=1}^{m_s}\sigma_j^2 + \sigma_s^2 + \sum_{i=1}^{m_t}\sigma_i^2 + \sigma_t^2. \tag{37}$$

Under this viewpoint, the conditional pdf $f_{Z|k}(z)$ is derived as follows (Remark 1).

$$f_{Z|k}(z) = \int_0^\infty P[Z|D=x]P[D=x|k]\mathrm{d}x \tag{38}$$

$$= \int_0^\infty \frac{z}{\sigma^2} e^{-\frac{x^2+z^2}{2\sigma^2}} I_0\left[\frac{zx}{\sigma^2}\right]\cdot\frac{2(\pi\lambda_B)^k}{\Gamma[k]}x^{2k-1}e^{-\pi\lambda_B x^2}\mathrm{d}x \tag{39}$$

$$= \frac{2(\pi\lambda_B)^k}{\sigma^2\Gamma[n]} z e^{-\frac{z^2}{2\sigma^2}}\cdot\int_0^\infty x^{2n-1}e^{-\frac{(2\pi\lambda\sigma^2+1)x^2}{2\sigma^2}} I_0\left[\frac{zx}{\sigma^2}\right]\mathrm{d}x \tag{40}$$

$$= \frac{1}{\sigma^2}\left(\frac{2\pi\lambda\sigma^2}{2\pi\lambda\sigma^2+1}\right)^k z e^{-\frac{\pi\lambda z^2}{2\pi\lambda\sigma^2+1}} \cdot L_{k-1}\left[-\frac{z^2}{2\sigma^2(2\pi\lambda\sigma^2+1)}\right] \tag{41}$$

$$Z = \sqrt{\left(D + \sum_{j=1}^{m_s} S_{j,x} + R_{s,x} - \sum_{i=1}^{m_t} T_{i,x} - R_{t,x}\right)^2 + \left(\sum_{i=1}^{m_t} T_{i,y} + R_{t,y} - \sum_{j=1}^{m_s} S_{j,y} - R_{s,y}\right)^2}. \tag{17}$$

$$Q_x = D + \sum_{j\in\mathcal{L}_s} S_j\cos\phi_j + \sum_{j\in\bar{\mathcal{L}}_s} S_{j,x} + R_{s,x} - \sum_{i\in\mathcal{L}_t} T_i\cos\theta_i + \sum_{i\in\bar{\mathcal{L}}_t} T_{i,x} - R_{t,x} \tag{18}$$

$$Q_y = \sum_{i\in\mathcal{L}_t} T_i\sin\theta_i + \sum_{i\in\bar{\mathcal{L}}_t} T_{i,y} + R_{t,y} - \sum_{j\in\mathcal{L}_s} S_j\sin\phi_j - \sum_{j\in\bar{\mathcal{L}}_s} S_{j,y} - R_{s,y}. \tag{19}$$

where $L_n[z]$ is the Laguerre polynomial, (39) is derived by substituting (1) and (3), (40) by rearranging (39), and (41) by solving the integral using [27, pp. 303] and elaborating with the result. We now turn our attention to the derivation of the respective ccdf $\bar{F}_{Z|k}(z)$.

$$\bar{F}_{Z|k}(z) = \int_{y=0}^{\infty} f_{D|k}(y)\bar{F}_{Z|D=y}(x)\mathrm{d}y \tag{42}$$

$$= \int_{y=0}^{\infty} \left(\frac{2(\pi\lambda)^k}{\Gamma[k]} y^{2k-1} e^{-\pi\lambda y^2}\right) \left(Q_1\left[\frac{y}{\sigma}, \frac{z}{\sigma}\right]\right) \mathrm{d}y \tag{43}$$

$$= \frac{e^{-\frac{\pi\lambda z^2}{2\pi\lambda\sigma^2+1}}}{2\pi\lambda\sigma^2+1} \sum_{n=0}^{k-1} \epsilon_n \left(\frac{2\pi\lambda\sigma^2}{2\pi\lambda\sigma^2+1}\right)^n \cdot L_n\left[-\frac{z^2}{2\sigma^2(2\pi\lambda\sigma^2+1)}\right], \tag{44}$$

where (43) follows from the law of total probability, (43) by substituting (27) and (1), and (45) by solving the integral using [29] for $\epsilon_n = 1, \forall n < k-1$ and $\epsilon_{k-1} = 2\pi\lambda\sigma^2 + 1$. The expressions in (10) and (11) are derived by plugging $\epsilon_{k-1} = 2\pi\lambda\sigma^2 + 1$ in (41) and (44), respectively.

C. Proof of Theorem 3

From Corollary 1, the distance Z is given by

$$z = g(D_n) \triangleq \sqrt{(D + Z_x)^2 + Z_y^2}, \tag{45}$$

where the parameters Z_x and Z_y are fixed and equal to (8) and (9), respectively. By taking a closer look to (45) it follows that the distance Z is always greater or equal to $|Z_y|$. Thus, $f_{Z|k,full} = 0$ for $Z < |Z_y|$. On the other hand, for $Z \geq |Z_y|$, the distance Z is a function of a single RV (the distance D) with known probability distribution (1). Therefore, for $z \geq |Z_y|$ the conditional pdf $f_{Z|k,full}$ can be derived as follows [26, pp. 93]:

$$f_{Z|k,full}(z) = \frac{f_D(d_1)}{|g'(d_2)|} + \frac{f_D(d_2)}{|g'(d_2)|}, \tag{46}$$

where $d_1 = -Z_x - \sqrt{z^2 - Z_y^2}$ and $d_2 = -Z_x + \sqrt{z^2 - Z_y^2}$ are the real roots of (45), and $g'(d)$ is the derivative of $g(d)$ in (45). Substituting $g'(d) = \frac{d+Z_x}{z}$ in (46), yields (12). Note that the unit step function $U[x]$ is used to ensure that the distance D is strictly positive. The ccdf $\bar{F}_{Z|k,full}(z)$ for $z \geq Z_y$ is derived by substituting d_1 and d_2 in (12), and integrating with respect to z we reach to (47) and (48), shown at the bottom of the page, where in (48) we have employed the change of variables $v = -Z_x - \sqrt{x^2 - Z_y^2}$ and $g = -Z_x + \sqrt{y^2 - Z_y^2}$. The ccdf in (13) is derived by solving the integrals in (49) and substituting $d_1 = -Z_x - \sqrt{z^2 - Z_y^2}$ and $d_2 = -Z_x + \sqrt{z^2 - Z_y^2}$.

D. Proof of Theorem 4

By combining Lemma 3 and Theorem 1, it can be shown that the PoP $\mathcal{A}_D$ is given by $\mathcal{A}_D = 1 - Q_1\left[\frac{\sqrt{\eta_x^2+\eta_y^2}}{\sigma}, \frac{1}{\sigma}\left(\frac{c}{Z_{th}}\right)^{\frac{1}{a}}\right]$. Let us now define the ratio $\zeta = \sqrt{\eta_x^2 + \eta_y^2}\left(\frac{c}{Z_{th}}\right)^{-\frac{1}{a}}$, which corresponds to the ratio of the arguments in the Marcum-Q function. By using the transform in [29, (4.16)] for $\zeta < 1$, we re-write the probability $\mathcal{A}_D$ as follows:

$$\mathcal{A}_D = 1 - \frac{1}{2\pi}\int_{-\pi}^{\pi} \frac{(1 + \zeta\sin\theta)e^{-\frac{\left(\frac{c}{Z_{th}}\right)^{\frac{2}{a}}}{2\sigma^2}(1+2\zeta\sin\theta+\zeta^2)}}{1 + 2\zeta\sin\theta + \zeta^2}\mathrm{d}\theta. \tag{49}$$

By plugging $\sigma^2 = \sigma_n^2 + \sigma_o^2$ in (49) and differentiating with respect to σ_o^2, we get:

$$\frac{\partial\mathcal{A}_D}{\partial\sigma_o^2} = -\frac{\left(\frac{c}{Z_{th}}\right)^{\frac{2}{a}}}{4\pi\left(\sigma_n^2+\sigma_o^2\right)^2} \cdot \int_{-\pi}^{\pi}(1+\zeta\sin\theta)e^{-\frac{\left(\frac{c}{Z_{th}}\right)^{\frac{2}{a}}}{2\left(\sigma_n^2+\sigma_o^2\right)}(1+2\zeta\sin\theta+\zeta^2)}\mathrm{d}\theta \tag{50}$$

$$= \frac{\left(\frac{c}{Z_{th}}\right)^{\frac{2}{a}}}{2\left(\sigma_n^2+\sigma_o^2\right)^2} e^{-\frac{\left(\frac{c}{Z_{th}}\right)^{\frac{2}{a}}}{2\left(\sigma_n^2+\sigma_o^2\right)}(1+z^2)} \cdot \left(\zeta I_1\left[\frac{\zeta\left(\frac{c}{Z_{th}}\right)^{\frac{2}{a}}}{\sigma_n^2+\sigma_o^2}\right] - I_0\left[\frac{\zeta\left(\frac{c}{Z_{th}}\right)^{\frac{2}{a}}}{\sigma_n^2+\sigma_o^2}\right]\right). \tag{51}$$

Since all parameters in (51) are positive real and by definition $I_0[x] > I_1[x]\ \forall x > 0$, the sign of (51) for $\zeta < 1$ is always negative. Therefore, the PoP $\mathcal{A}_D$ decreases with σ_o^2 when $\zeta < 1$.

$$\bar{F}_{Z|k,full}(z) = \int_z^{\infty} \frac{2(\pi\lambda)^k}{\Gamma[k]} \frac{x}{\sqrt{x^2 - Z_y^2}} \frac{\left(-Z_x - \sqrt{x^2 - Z_y^2}\right)^{2k-1} U\left[\left(-Z_x - \sqrt{x^2 - Z_y^2}\right)\right]}{e^{\pi\lambda\left(-Z_x - \sqrt{x^2-Z_y^2}\right)^2}}\mathrm{d}x + \int_z^{\infty} \frac{2(\pi\lambda)^n}{\Gamma[n]} \frac{y}{\sqrt{y^2 - Z_y^2}} \frac{\left(-Z_x + \sqrt{y^2 - Z_y^2}\right)^{2k-1} U\left[\left(-Z_x + \sqrt{y^2 - Z_y^2}\right)\right]}{e^{\pi\lambda\left(-Z_x + \sqrt{y^2-Z_y^2}\right)^2}}\mathrm{d}y \tag{47}$$

$$= -\int_{-\infty}^{-Z_x - \sqrt{z^2-Z_y^2}} \frac{2(\pi\lambda)^k}{\Gamma[k]} \frac{v^{2k-1}U[v]}{e^{\pi\lambda v^2}}\mathrm{d}v + \int_{-Z_x + \sqrt{z^2-Z_y^2}}^{\infty} \frac{2(\pi\lambda)^k}{\Gamma[k]} \frac{g^{2k-1}U[g]}{e^{\pi\lambda g^2}}\mathrm{d}g, \tag{48}$$

We now examine the monotonicity of $\mathcal{A}_D$ when $\zeta > 1$. For notational convenience, we use the parameter $q = \frac{1}{\zeta}$. By using the transform in [29, (4.19)], the probability $\mathcal{A}_D$ can be re-written as follows:

$$\mathcal{A}_D = -\frac{1}{2\pi}\int_{-\pi}^{\pi} \frac{(q^2+q\sin\theta)e^{-\frac{\eta_x^2+\eta_y^2}{2\left(\sigma_n^2+\sigma_o^2\right)}(1+2q\sin\theta+q^2)}}{1+2q\sin\theta+q^2}\mathrm{d}\theta. \tag{52}$$

By following a similar methodology with the one used for (52), we reach to

$$\frac{\partial \mathcal{A}_D}{\partial \sigma_o^2} = \frac{q\left(\eta_x^2+\eta_y^2\right)}{2\left(\sigma_n^2+\sigma_o^2\right)^2} e^{-\frac{\left(1+q^2\right)\left(\eta_x^2+\eta_y^2\right)}{2\left(\sigma_n^2+\sigma_o^2\right)}} \cdot \left(I_1\left[\frac{q\left(\eta_x^2+\eta_y^2\right)}{\sigma_n^2+\sigma_o^2}\right] - qI_0\left[\frac{q\left(\eta_x^2+\eta_y^2\right)}{\sigma_n^2+\sigma_o^2}\right]\right). \tag{53}$$

Since all parameters in (53) are positive real, $I_0[x] > I_1[x]$ $\forall x > 0$, and $q = \frac{1}{\zeta} < 1$, there exists an optimal variance parameter σ_o^{2*} for which the weighted difference of the Bessel functions is equal to zero. The optimal σ_o^{2*} satisfies $\frac{\partial \mathcal{A}_D}{\partial \sigma_o^{2*}} = 0$, which is equivalent to (14). By employing the approximations $I_0[x] = \frac{e^x}{\sqrt{2\pi x}}\left(1+\frac{1}{8x}\right)$ and $I_1[x] = \frac{e^x}{\sqrt{2\pi x}}\left(1-\frac{3}{8x}\right)$ in (14), we reach to (15).

REFERENCES

[1] H. S. Dhillon, R. K. Ganti, F. Baccelli, and J. G. Andrews, "Modeling and analysis of *K*-tier downlink heterogeneous cellular networks," *IEEE J. Sel. Areas Commun.*, vol. 30, no. 3, pp. 550–560, Mar. 2012.

[2] *Part 11: Wireless LAN Medium Access Control (MAC) and Physical Layer (PHY) Specifications*, IEEE Std. 802.11-2012 (Revision of IEEE 802.11-2007), Mar. 2012.

[3] *Part 15.4: Low-Rate Wireless Personal Area Networks (LR-WPANs)*, IEEE Std. 802.15.4 (Revision of IEEE Std. 802.15.4-2006), Jun. 2011.

[4] Y. Yan, Y. Qian, H. Sharif, and D. Tipper, "A survey on smart grid communication infrastructures: Motivations, requirements and challenges," *IEEE Commun. Survey Tuts.*, vol. 15, no. 1, pp. 5–20, 1st Quart. 2013.

[5] J. G. Andrews, R. K. Ganti, M. Haenggi, N. Jindal, and S. Weber, "A primer on spatial modeling and analysis in wireless networks," *IEEE Commun. Mag.*, vol. 48, no. 11, pp. 156–163, Nov. 2010.

[6] R. K. Ganti and M. Haenggi, "Interference and outage in clustered wireless ad hoc networks," *IEEE Trans. Inf. Theory*, vol. 55, no. 9, pp. 4067–4086, Sep. 2009.

[7] G. Alfano, M. Garetto, and E. Leonardi, "Capacity scaling of wireless networks with inhomogeneous node density: Upper bounds," *IEEE J. Sel. Areas Commun.*, vol. 27, no. 7, pp. 1147–1157, Sep. 2009.

[8] R. Verdone, F. Fabbri, and C. Buratti, "Maximizing area throughput in clustered wireless sensor networks," *IEEE J. Sel. Areas Commun.*, vol. 28, no. 7, pp. 1200–1210, Sep. 2010.

[9] Y. Zhong and W. Zhang, "Multi-channel hybrid access femtocells: A stochastic geometric analysis," *IEEE Trans. Commun.*, vol. 61, no. 7, pp. 3016–3026, Jul. 2013.

[10] 3GPP, "Physical layer—Measurements," Eur. Telecommun. Stand. Instit., Sophia-Antipolis Cedex, France, TS 36.214 V11.1.0, Dec. 2012.

[11] S. Marano, W. M. Gifford, H. Wymeersch, and M. Z. Win, "NLOS identification and mitigation for localization based on UWB experimental data," *IEEE J. Sel. Areas Commun.*, vol. 28, no. 7, pp. 1026–1035, Sep. 2010.

[12] G. Giorgetti, S. K. S. Gupta, and G. Manes, "Understanding the limits of RF-based collaborative localization," *IEEE/ACM Trans. Netw.*, vol. 19, no. 6, pp. 1638–1651, Dec. 2011.

[13] A. Kupper, *Location-Based Services: Fundamentals and Operation*. New York, NY, USA: Wiley, 2005.

[14] J. Ni, R. Srikant, and X. Wu, "Coloring spatial point processes with applications to peer discovery in large wireless networks," *IEEE/ACM Trans. Netw.*, vol. 19, no. 2, pp. 575–588, Apr. 2011.

[15] T. Kwon and J. Choi, "Spatial performance analysis and design principles for wireless peer discovery," *IEEE Trans. Wireless Commun.*, vol. 13, no. 8, pp. 4507–4519, Aug. 2014.

[16] Y. Li, F. Baccelli, H. Dhillon, and J. Andrews, "Statistical modeling and probabilistic analysis of cellular networks with determinantal point processes," *IEEE Trans. Commun.*, arXiv preprint arXiv:1412.2087, 2014.

[17] X. Lin, J. G. Andrews, A. Ghosh, and R. Ratasuk, "An overview of 3GPP device-to-device proximity services," *IEEE Commun. Mag.*, vol. 52, no. 4, pp. 40–48, Apr. 2014.

[18] Y. Yan and Y. Mostofi, "Co-optimization of communication and motion planning of a robotic operation under resource constraints and in fading environments," *IEEE Trans. Wireless Commun.*, vol. 12, no. 4, pp. 1562–1572, Apr. 2013.

[19] M. Hosan, E. Hossain, and D. Niyato, "Random access for machine-to-machine communication in LTE-Advanced networks: Issues and approaches," *IEEE Commun.*, vol. 51, no. 6, pp. 86–93, Jun. 2013.

[20] M. A. Alsheikh, S. Lin, D. Niyato, and H.-P. Tan, "Machine learning in wireless sensor networks: Algorithms, strategies and applications," *IEEE Commun. Surveys Tuts.*, vol. 16, no. 4, pp. 1996–2018, 4th Quart. 2014.

[21] J. G. Andrews *et al.*, "What will 5G be?" *IEEE J. Sel. Areas Commun.*, vol. 32, no. 6, pp. 1065–1082, Jul. 2014.

[22] G. Garcia, S. Muppirisetty, E. Schiller, and H. Wymeersch, "On the trade-off between accuracy and delay in cooperative UWB localization: Performance bounds and scaling laws," *IEEE Trans. Wireless Commun.*, vol. 13, no. 8, pp. 4574–4585, Aug. 2014.

[23] M. Haenggi, "On distances in uniformly random networks," *IEEE Trans. Inf. Theory*, vol. 51, no. 10, pp. 3584–3586, Oct. 2005.

[24] R. Peng and M. L. Sichitiu, "Angle of arrival localization for wireless sensor networks," in *Proc. IEEE Commun. Soc. SECON*, Sep. 2006, pp. 374–382.

[25] A. Guo and M. Haenggi, "Asymptotic deployment gain: A simple approach to characterize the SINR Distribution in general cellular networks," *IEEE Trans. Commun.*, vol. 63, no. 3, pp. 962–976, Mar. 2015.

[26] A. Papoulis, *Probabilities, Random Variables and Stochastic Processes*, 3rd ed. New York, NY, USA: McGraw-Hill, 1991.

[27] A. P. Prudnikov, Y. A. Brychkov, and O. I. Marichev, *Integrals and Series: Special Functions*, vol. 2. London, U.K.: CRC Press, 1986.

[28] A. H. Nuttall, "Some integrals involving the Q_M function," *IEEE Trans. Inf. Theory*, vol. 21, no. 1, pp. 95–96, Jan. 1975.

[29] M. K. Simon and M. S. Alouini, *Digital Communication Over Fading Channels: A Unified Approach to Performance Analysis*. New York, NY, USA: Wiley-Interscience, 2000.

Dionysis Xenakis received the B.Sc. degree in computer science in 2007 and the M.Sc. degree in communications systems and networks in 2009. He has been pursuing the Ph.D. degree at the Department of Informatics and Telecommunications—University of Athens, Greece. In 2008, he received the M.Sc. Excellence Award in the field of networks and communication systems from the same department. He participated in various FP7 research projects, including PHYDYAS, C2POWER, HRAKLEITOS II, CROSSFIRE, and SMART-NRG. He is a co-author of 12 conference papers, six journals papers, and four book chapters. Among others, he has served as a reviewer in numerous peer-reviewed journals and has been a technical program committee member in top international conferences including IEEE ICC 2015 and 2016, IEEE GLOBECOM 2015, IEEE CAMAD 2014–2016, and IEEE HealthCom 2014–2015. He has given numerous training seminars under various EU-funded projects, such as BeFEMTO, FREEDOM, CROSSFIRE, ACROPOLIS, WHERE2, and SMART-NRG. His current research interests are in the area of mobile cellular communications, advanced localization techniques and spatial modeling for wireless networks. He is currently an Associate Researcher in the Green Adaptive and Intelligent Networking Group (GAIN) at the University of Athens—Greece.

Lazaros Merakos received the Diploma in electrical and mechanical engineering from the National Technical University of Athens, Athens, Greece, in 1978, and the M.S. and Ph.D. degrees in electrical engineering from the State University of New York, Buffalo, NY, USA, in 1981 and 1984, respectively. From 1983 to 1986, he was on the faculty of the Electrical Engineering and Computer Science Department, University of Connecticut, Storrs, CT, USA. From 1986 to 1994, he was on the faculty of the Electrical and Computer Engineering Department, Northeastern University, Boston, MA, USA. During the period 1993–1994, he served as Director of the Communications and Digital Signal Processing Research Center, Northeastern University. During the summers of 1990 and 1991, he was a Visiting Scientist at the IBM T. J. Watson Research Center, Yorktown Heights, NY. In 1994, he joined the faculty of the University of Athens, Athens, Greece, where he is presently a Professor in the Department of Informatics and Telecommunications and Director of the Communication Networks Laboratory (UoA-CNL). Since 1994, he has led the participation of UoA-CNL in several of the key research projects that have shaped European R&D in the area of wireless/mobile networks, including the EU funded projects RAINBOW, WAND, MOBIVAS, WINE, ANWIRE, E2R, E2RII, E3, Self-NET and SACRA. His research interests are in the design and performance analysis of communication networks, and wireless/mobile communication systems and services. He has authored more than 250 papers in the above areas. He is a member of the board of the National Research Network of Greece, and chairman of the board of the Greek Universities Network (GUNet), a non-profit organization for the coordinated introduction of advanced ICT and e-learning services for the Greek academic community.

Marios Kountouris (S'04–M'08–SM'15) received the Diploma in electrical and computer engineering from the National Technical University of Athens, Greece, in 2002 and the M.S. and Ph.D. degrees in electrical engineering from the Ecole Nationale Supérieure des Télécommunications (Télécom ParisTech), France, in 2004 and 2008, respectively. His doctoral research was carried out at Eurecom Institute, France, and it was funded by Orange Labs, France. From February 2008 to May 2009, he was with the Department of ECE, The University of Texas at Austin as a Research Associate, working on wireless ad hoc networks under DARPA's IT-MANET program. From June 2009 to December 2013, he was an Assistant Professor at the Department of Telecommunications, Supélec (Ecole Supérieure d'Electricité), France, where he is currently an Associate Professor. From March 2014 to February 2015, he was an Adjunct Professor in the School of EEE, Yonsei University, S. Korea. Since January 2015, he has been a Principal Researcher at the Mathematical and Algorithmic Sciences Lab, Huawei Technologies, France.

Dr. Kountouris has published several papers and patents all in the area of communications, wireless networks, and signal processing. He has served as technical program committee member for several top international conferences and has served as Workshop Chair for the IEEE Globecom 2010 Workshop on Femtocell Networks, the IEEE ICC 2011 Workshop on Heterogeneous Networks, and the IEEE Globecom 2012 Workshop on Heterogeneous and Small Cell Networks.

He is currently an Editor for the IEEE TRANSACTIONS ON WIRELESS COMMUNICATIONS, the *EURASIP Journal on Wireless Communications and Networking*, and the *Journal of Communications and Networks (JCN)*. He is also a founding member and Vice Chair of IEEE SIG on Green Cellular Networks. He received the 2013 IEEE ComSoc Outstanding Young Researcher Award for the EMEA Region, the 2014 EURASIP Best Paper Award for EURASIP Journal on Advances in Signal Processing (JASP), the 2012 IEEE SPS Signal Processing Magazine Award, the IEEE SPAWC 2013 Best Student Paper Award, and the Best Paper Award in Communication Theory Symposium at IEEE Globecom 2009. He is a Professional Engineer of the Technical Chamber of Greece.

Nikos Passas received the Diploma (honors) from the Department of Computer Engineering, University of Patras, Greece, and the Ph.D. degree from the Department of Informatics and Telecommunications, University of Athens, Greece, in 1992 and 1997, respectively. Since 1995, he has been with the Communication Networks Laboratory, University of Athens, working as a Lecturer and Senior Researcher in a number of national and European research projects. He has also served as a guest editor and technical program committee member in prestigious magazines and conferences, such as *IEEE Wireless Communications Magazine*, IEEE VTC, IEEE PIMRC, IEEE Globecom, etc. He has published more than 100 papers in peer-reviewed journals and international conferences and has also published 1 book and 10 book chapters. His research interests are in the area of mobile network architectures and protocols.

Christos Verikoukis received the Ph.D. degree from UPC in 2000. He is currently a Senior Researcher at CTTC and an Adjunct Professor at the University of Barcelona. His area of expertise is in the design of energy-efficient layer 2 protocols and RRM algorithms for short-range wireless cooperative and network coded communications. He has published 80 journal papers and over 160 conference papers. He is also a co-author of three books, 14 chapters in other books, and two patents. He has participated in more than 30 competitive projects, and has served as the principal investigator of national projects in Greece and Spain as well as the technical manager of Marie-Curie and Celtic projects. He has supervised 15 Ph.D. students and five postdoctoral researchers since 2004. He was General Chair of the 17th, 18th, and 19th IEEE CAMAD, the TPC Chair of the 6th IEEE Latincom, and TPC Co-Chair of the 15th Healthcom. He has also served as the CQRM symposium co-chair in the IEEE Globecom 2014 and IEEE ICC 2015 & 2016. He is currently the Chair of the IEEE ComSoc Technical Committee on Communication Systems Integration and Modeling. He received the Best Paper Award of the Communication QoS, Reliability & Modeling Symposium in IEEE ICC 2011 and in Selected Areas in Communications Symposium of the IEEE Globecom 2014 as well as the EURASIP 2013 Best Paper Award for the Journal on Advances in Signal Processing.